Engineering Analysis with Boundary Elements 128 (2021) 298–309

Contents lists available at ScienceDirect

Engineering Analysis with Boundary Elements

journal homepage: www.elsevier.com/locate/enganabound

IG-DRBEM of three-dimensional transient heat conduction problems

Bo Yu [a], Geyong Cao [a], Yanpeng Gong [b,*], Shanhong Ren [a], Chunying Dong [c]

[a] School of Civil Engineering, Hefei University of Technology, Hefei 230009, P.R. China
[b] Institute of Electronics Packaging Technology and Reliability, Faculty of Materials and Manufacturing, Beijing University of Technology, Beijing, 100124, P.R. China
[c] Department of Mechanics, School of Aerospace Engineering, Beijing Institute of Technology, Beijing, 100081, P.R. China

ARTICLE INFO

Keywords:
Isogeometric BEM
Dual reciprocity method
3D transient heat transfer

ABSTRACT

In this paper, the isogeometric dual reciprocity boundary element method (IG-DRBEM) is proposed to solve three-dimensional transient heat conduction problems. It is well known that the error of traditional BEM mainly comes from element dispersion, and the introduction of isogeometric ideas makes BEM become a veritable high-precision numerical method. At present, most of the problems solved by isogeometric BEM (IGBEM) are time-independent. The reason is similar to the traditional BEM, which cannot avoid solving domain integrals when solving time-dependent problems. In this paper, based on the potential fundamental solution the boundary-domain integral equation is obtained by the weighted residual method, where the classic dual reciprocity method is adopted to transform domain integrals into boundary integrals. Meanwhile, a two-level time integration scheme is used to solve the discretized differential equations. In addition, the adaptive integration scheme, the radial integral transform method and the power series expansion method are adopted to solve the boundary regular, nearly singular and singular integrals. Several classical numerical examples show that the presented method has good numerical stability and high precision by considering different factors such as the approximation function, the time step, the number of interior points and so on.

1. Introduction

Since the isogeometric analysis method based on the finite element was proposed by Hughes et al. [1], many isogeometric methods were formed by combining with other numerical methods, such as the isogeometric collocation method [2], the isogeometric meshless finite volume method [3], the scaled boundary isogeometric finite element method [4,5] and the isogeometric boundary element method (IGBEM) [6]. IGBEM has all the advantages of the traditional boundary element method (BEM). Up to now, the IGBEM has been widely applied in many fields. For example, the IGBEM based on the Non-Uniform Rational B-Splines (NURBS) solves the two-dimensional linear elastostatic problem [6]. And in 2013, Scott et al. [7] improved the IGBEM by using the unstructured T-splines as the basis function to analyze the three-dimensional linear elastostatic problem. Meanwhile, Peake et al. [8] presented the extended isogeometric boundary element method to solve the two-dimensional Helmholtz problem. Similar to the traditional BEM, Takahashi and Matsumoto [9] introduced the fast multipole method into IGBEM to solve the large-scale problem. More recently, the IGBEM was successfully applied to solve the crack problem [10,11], the heat transfer problem [12] and the shape optimization problem [13]. It is worth noting that these problems are time-independent. Based on this, the three-dimensional (3D) transient heat transfer problem will be solved by the IGBEM in this work.

Generally, the domain integral is inevitable when we use BEM to solve the transient heat transfer problem with heat sources. In order to maintain the advantage of dimensionality reduction, the domain integral needs to be transformed into the boundary integral. In recent decades, many scholars proposed some transformation methods of domain integrals, where the dual reciprocity method (DRM) [14] and the radial integration method (RIM) [15] are two commonly used transformation methods. Comparing with the RIM which was proposed by Gao in 2002, the DRM which was proposed by Nardini and Brebbia in 1982 has the advantage of programming simple and easy implementation. The dual reciprocity BEM (DRBEM) is formed by introducing DRM into BEM. Up to now, DRBEM has been widely used to solve the nonlinear diffusion problem [16], the thermal wave propagation in biological tissues [17], the dynamic crack problem [18], the transient heat transfer problem [19], the elastoplastic problem [20] and so on. More recently, Yu et al. [21] proposed the isogeometric DRBEM (IG-DRBEM) to solve the 2D transient heat conduction problem. In this paper, a new theoretical framework for solving 3D transient heat transfer problems with

Abbreviations: Abserr, absolute error; BEM, boundary element method; DRM, dual reciprocity method; IGBEM, isogeometric boundary element method; Mabserr, maximum absolute error; Mrelerr, maximum relative error; NURBS, non-uniform rational B-spline; Relerr, relative error; RIM, radial integration method.

* Corresponding author.
E-mail address: yanpeng.gong@bjut.edu.cn (Y. Gong).

https://doi.org/10.1016/j.enganabound.2021.04.014
Received 22 December 2020; Received in revised form 7 April 2021; Accepted 16 April 2021

Nomenclature

c	specific heat
f_j	DRM expanding basis function
g	heat source
k	thermal conductivity
$\mathbf{n}$	normal vector
P	control point
p, q	order of NURBS basis functions
Q	heat flux
r	distance between two points
$\mathbf{R}$	NURBS basis function matrix
S	NURBS surface
t	time
T	temperature
T^*	fundamental solution
x_1,x_2,x_3	Cartesian coordinate of $\mathbf{x}$

Greek symbols

α	DRM time-dependent coefficient
Γ	boundary of the problem domain
ρ	density
θ_T,θ_Q,θ_g	linear approximate parameter
λ	$k/\rho c$
ω	weight of control point
Ω	domain of problem

Superscripts

e'	source point element
s	s-th time interval
T	transpose of vector

Subscripts

AI	newly added internal point
b	boundary collocation point
I	interior point
m	number of basis functions in ξ direction
n	number of basis functions in η direction

IG-DRBEM will be established based on the 3D steady potential theory of literature [22].

It is worth noting that when we use IGBEM to analyze the problem, only a few elements are generally needed to accurately describe the real geometry and obtain high precision numerical results. Therefore, the size of an isogeometric boundary element will be much larger than a traditional boundary element. For the regular integral, to obtain accurate numerical integral results many Gauss integral points need to be used. But this scheme will increase the computational cost rapidly. To improve the computational efficiency, Gao and Davies [23] presented an adaptive integration method that can automatically choose the optimal Gauss integration points. In the computation process, if the number of required Gauss integration points exceeds the maximum, the integration elements will be divided into sub-elements. In 2017, Gong and Dong [24] adopted this scheme to analyze the three-dimensional steady potential problem. Although the size of isogeometric elements is generally big, the near singular and singular integrals are also inevitable. For example, the nearly singular and singular integrals will respectively appear when the computed points are very close to the real boundary of the model and when the computed points locate on the same element as the other field points, i.e. the case of distance variable $r = 0$ occurs. There are many methods [25,26,27] to deal with the nearly singular integrals in conventional BEM. These methods fail when solving some complex computational models [28]. In literature [24], the adaptive integration method has been verified to be effective in dealing with the nearly singular integrals in IGBEM. For the singular integrals, over the past two decades, many researchers proposed various algorithms [29,30,31,32] to analyze this problem. In 2012, the self-adaptive coordinate transformation method [29] was used to solve the singular integral in IGBEM [6]. However, this method may be arduous and computationally expensive. In 2017, Gong and Dong [24] adopted the power series expansion method [33] to solve the three-dimensional singular integral in IGBEM. The literature [24] focuses on the research of nearly singular and singular integrals for the 3D steady potential problem in 3D IGBEM. In this paper, by coupling DRM and IGBEM (approach abbreviated as IG-DRBEM), we will extend the 3D steady potential problem to the 3D transient heat transfer problem with heat sources in IGBEM. To the authors' knowledge, up to date, it is the first implementation of IG-DRBEM to solve 3D transient heat transfer problems in the literature.

The paper is organized as follows. The governing equation and the definition of the problem are introduced in Section 2. NURBS basis functions are described in Section 3. The isogeometric dual reciprocity BEM is elaborated in Section 4. Then, three typical numerical examples are discussed in Section 5. Finally, the conclusions are summarized in Section 6.

2. Governing equation

In this paper, a 3D bounded domain Ω with boundary $\Gamma=\partial\Omega$, occupied by the isotropic material with constant material parameters. The governing equation for the transient heat conduction problem can be expressed as [34]

$$k\nabla^2 T(\mathbf{x},t) + g(\mathbf{x},t) = \rho c \frac{\partial T(\mathbf{x},t)}{\partial t}, \mathbf{x} \in \Omega \tag{1}$$

where $\mathbf{x} = (x_1,x_2,x_3)$ is a point in the domain Ω, ∇^2 is the Laplace operator, $T(\mathbf{x}, t)$ is the temperature at the point $\mathbf{x}$ at time t, $g(\mathbf{x}, t)$ is a known heat source function, k is the thermal conductivity, ρ is the density and c is the specific heat.

The temperature and heat flux boundary conditions are considered, namely

$$T(\mathbf{x},t)=\bar{T}(\mathbf{x},t), \mathbf{x} \in \Gamma_1 \tag{2}$$

and

$$-k\frac{\partial T}{\partial \mathbf{n}} = \bar{\mathrm{Q}}(\mathbf{x},t), \mathbf{x} \in \Gamma_2 \tag{3}$$

where $\Gamma_1 \cup \Gamma_2=\Gamma, \Gamma_1 \cap \Gamma_2=\emptyset$, $\bar{T}$ and $\bar{\mathrm{Q}}$ denote the known temperature and heat flux, respectively. $\mathbf{n}$ is the outward normal vector of the boundary Γ. Generally, the initial condition is given by

$$T(\mathbf{x},0)=T_0(\mathbf{x}) \tag{4}$$

3. NURBS basis functions

In this paper, NURBS is adopted to approximate field variables and describe the geometry surface [24]. Here we briefly recall the main definitions. Firstly, two knot vectors are defined by the non-decreasing sequence of coordinates in the parametric space:

$$\Xi=\{\xi_1, \xi_2, \cdots, \xi_{n+p+1}\} \tag{5}$$

$$\Pi=\{\eta_1,\eta_2, \cdots, \eta_{m+q+1}\} \tag{6}$$

where n and m are respectively the number of basis functions along the two parametric directions ξ and η, p and q are the corresponding polynomial orders. The parameter space can be split into knot spans, which are considered as elements in isogeometric analysis. The bivariate basis functions $R_{i,j}^{p,q}(\xi,\eta)$ are given by

$$R_{i,j}^{p,q}(\xi,\eta) = \frac{N_{i,p}(\xi)M_{j,q}(\eta)\omega_{i,j}}{\sum_{\hat{i}=1}^{n}\sum_{\hat{j}=1}^{m} N_{\hat{i},p}(\xi)M_{\hat{j},q}(\eta)\omega_{\hat{i},\hat{j}}} \tag{7}$$

where $N_{i,p}$ and $M_{j,q}$ are the i-th B-spline basis function of order p and the j-th B-spline basis function of order q, respectively. $\omega_{i,j}$ represents

the weight value corresponding to the control point $P_{i,j}$. The B-Spline basis functions $N_{i,p}(\xi)$ are defined recursively as follows:

$$N_{i,0} = \begin{cases} 1 & \text{if} \quad \xi_i \le \xi < \xi_{i+1} \\ 0 & \text{otherwise} \end{cases} \tag{8}$$

and for $p \ge 1$

$$N_{i,p}(\xi) = \frac{\xi - \xi_i}{\xi_{i+p} - \xi_i} N_{i,p-1}(\xi) + \frac{\xi_{i+p+1} - \xi}{\xi_{i+p+1} - \xi_{i+1}} N_{i+1,p-1}(\xi) \tag{9}$$

where $1 \le i \le n$, n is the number of basis functions to form the B-spline.

A tensor-product NURBS surface can be expressed as

$$S(\xi,\eta) = \sum_{i=1}^{n}\sum_{j=1}^{m} R_{i,j}^{p,q}(\xi,\eta) P_{i,j} \tag{10}$$

4. Isogeometric dual reciprocity BEM

In this section, before introducing the IG-DRBEM, we need to derive the dual reciprocity boundary integral equation with a heat source for three-dimensional transient heat conduction problems. Then the field variables and geometric surfaces are discretized by NURBS to form the IG-DRBEM.

4.1. Dual reciprocity boundary integral equation

In order to facilitate the use of DRM, Eq. (1) needs to be rewritten as

$$\nabla^2 T(\mathbf{x},t) = \tilde{b}(\mathbf{x},t) \tag{11}$$

where

$$\tilde{b}(\mathbf{x},t) = \frac{1}{\lambda}\frac{\partial T(\mathbf{x},t)}{\partial t} - \frac{g(\mathbf{x},t)}{k} \tag{12}$$

in which $\lambda = k/\rho c$. $\tilde{b}$ in Eq. (11) is approximated by a set of N_t functions $\{f_j(\mathbf{x})\}_{j=1}^{N_t}$ and the corresponding time-dependent coefficients $\{\alpha_j(t)\}_{j=1}^{N_t}$ as

$$\tilde{b}(\mathbf{x},t) = \sum_{j=1}^{N_t} \alpha_j(t) f_j(\mathbf{x}) \tag{13}$$

where for each known function $f_j(\mathbf{x})$ there exists a function $\hat{T}_j(\mathbf{x})$ such that $\nabla^2 \hat{T}_j(\mathbf{x}) = f_j(\mathbf{x})$. There are many kinds of functions $f_j(\mathbf{x})$ that have been investigated in the literature [14]. In this work, the polynomial function is adopted as follows:

$$f_j(\mathbf{x}) = 1 + r_j + r_j^2 + \cdots + r_j^a \tag{14}$$

where $r_j = \|\mathbf{x} - \mathbf{x}_j\|$ denotes the distance from the point $\mathbf{x}$ to the point $\mathbf{x}_j$.

Then

$$\hat{T}_j(\mathbf{x}) = \frac{r_j^2}{6} + \frac{r_j^3}{12} + \cdots + \frac{r_j^{a+2}}{(a+2)(a+3)} \tag{15}$$

In the following sections, we will also need

$$\hat{Q}_j = \frac{\partial \hat{T}_j(\mathbf{x})}{\partial \mathbf{n}} = \left(r_{jx_1}\frac{\partial x_1}{\partial \mathbf{n}} + r_{jx_2}\frac{\partial x_2}{\partial \mathbf{n}} + r_{jx_3}\frac{\partial x_3}{\partial \mathbf{n}}\right)\left(\frac{1}{3} + \frac{r_j}{4} + \cdots + \frac{r_j^a}{a+3}\right) \tag{16}$$

where r_{jx_1}, r_{jx_2}, and r_{jx_3} are the x_1, x_2, and x_3 components of r_j.

Applying the fundamental solution of steady potential problem $T^* = \frac{1}{4\pi r}$ to multiply Eq. (11) and integrating over the whole domain, the integral equation can be given by

$$\int_\Omega \left(\nabla^2 T(\mathbf{x},t)\right) T^* \mathrm{d}\Omega = \sum_{j=1}^{N_t} \alpha_j(t) \int_\Omega \left(\nabla^2 \hat{T}_j(\mathbf{x})\right) T^* \mathrm{d}\Omega \tag{17}$$

Integrating Eq. (17) by parts, the integral equation for any source point $\mathbf{x}'$ can be obtained with only boundary integrals as follows

$$\begin{aligned} &C(\mathbf{x}')T(\mathbf{x}') + \int_\Gamma T(\mathbf{x})Q^*(\mathbf{x}',\mathbf{x})\mathrm{d}\Gamma - \int_\Gamma q(\mathbf{x})T^*(\mathbf{x}',\mathbf{x})\mathrm{d}\Gamma \\ &= \sum_{j=1}^{N_t} \alpha_j \left[C(\mathbf{x}')\hat{T}_j(\mathbf{x}') + \int_\Gamma \hat{T}_j(\mathbf{x})Q^*(\mathbf{x}',\mathbf{x})\mathrm{d}\Gamma - \int_\Gamma \hat{Q}_j(\mathbf{x})T^*(\mathbf{x}',\mathbf{x})\mathrm{d}\Gamma\right] \end{aligned} \tag{18}$$

where $C(\mathbf{x}')$ is a jump term in which it can be obtained similar to the conventional BEM [35], Q^* is the normal derivative of the fundamental solution T^* along the boundary Γ and $Q^* = \partial T^*/\partial \mathbf{n}$.

Eq. (18) is the boundary integral equation obtained by the DRM. It is worth noting that Eq. (18) does not include any domain integrals, and the forms on the right and left sides of the equation are very similar, which can be embodied in the formation of the coefficient matrix later. In order to ensure the accuracy of the solution, a few points will be distributed into the interior of the domain as well as some nodes on the boundary. Finally, the unknown quantities of the boundary nodes and the points in the domain are solved simultaneously.

4.2. Isogeometric approximation by NURBS

Similar to Eq. (10), $\mathbf{x}$, T, Q, $\hat{T}_v$ and $\hat{Q}_v$ can also be expressed as

$$\begin{cases} \mathbf{x}(\xi,\eta) = \sum_{i=1}^{n}\sum_{j=1}^{m} R_{i,j}^{p,q}(\xi,\eta)\mathbf{x}_{i,j} \\ T(\xi,\eta) = \sum_{i=1}^{n}\sum_{j=1}^{m} R_{i,j}^{p,q}(\xi,\eta)T_{i,j} \\ Q(\xi,\eta) = \sum_{i=1}^{n}\sum_{j=1}^{m} R_{i,j}^{p,q}(\xi,\eta)Q_{i,j} \\ \hat{T}_v(\xi,\eta) = \sum_{i=1}^{n}\sum_{j=1}^{m} R_{i,j}^{p,q}(\xi,\eta)\hat{T}_{u_{i,j}v} \\ \hat{Q}_v(\xi,\eta) = \sum_{i=1}^{n}\sum_{j=1}^{m} R_{i,j}^{p,q}(\xi,\eta)\hat{Q}_{u_{i,j}v} \end{cases} \tag{19}$$

In the first three formulas of Eq. (19), $\mathbf{x}_{i,j}$, $T_{i,j}$, and $Q_{i,j}$ are the so-called control variables. In the last two formulas of Eq. (19), the left side is the function values of the distance from the point with parameter (ξ, η) to point v. On the right side, $\hat{T}_{u_{i,j}v}$ and $\hat{Q}_{u_{i,j}v}$ represent the control variables corresponding to the function values of the distance between point u and point v.

In 3D IGBEM analysis, two sets of knot vectors in different directions (ξ and η direction) constitute the knot vector space, and the different values of the two sets of knot vectors divide the knot vector space into non-overlapping subspaces. These subspaces are projected into physical coordinates, and the boundary Γ is divided into N_e surface elements. Also, the conditions need to be satisfied as $\Gamma = \bigcup_{e=1}^{N_e} \Gamma_e, \Gamma_i \cap \Gamma_j = \emptyset, i \ne j$. To facilitate numerical integration, we need to convert the coordinate of the element (ξ, η) to the local standard coordinate $(\hat{\xi}, \hat{\eta})$ so that $\hat{\xi} \in [-1, 1]$, $\hat{\eta} \in [-1, 1]$. Assuming the nodal vector interval at the e-th element is expressed as $[\xi_e, \xi_{e+1}]$ and $[\eta_e, \eta_{e+1}]$. The Jacobian of transformation $J^e(\hat{\xi}, \hat{\eta})$ is given by [24]

$$J^e(\hat{\xi},\hat{\eta}) = \frac{\mathrm{d}\Gamma}{\mathrm{d}\xi \mathrm{d}\eta}\frac{\mathrm{d}\xi \mathrm{d}\eta}{\mathrm{d}\hat{\xi}\mathrm{d}\hat{\eta}} \tag{20}$$

where

$$\begin{aligned} \frac{\mathrm{d}\Gamma}{\mathrm{d}\xi \mathrm{d}\eta} = \Bigg[&\left(\frac{\partial x_2}{\partial \xi}\frac{\partial x_3}{\partial \eta} - \frac{\partial x_3}{\partial \xi}\frac{\partial x_2}{\partial \eta}\right)^2 + \left(\frac{\partial x_3}{\partial \xi}\frac{\partial x_1}{\partial \eta} - \frac{\partial x_1}{\partial \xi}\frac{\partial x_3}{\partial \eta}\right)^2 \\ &+ \left(\frac{\partial x_1}{\partial \xi}\frac{\partial x_2}{\partial \eta} - \frac{\partial x_2}{\partial \xi}\frac{\partial x_1}{\partial \eta}\right)^2\Bigg]^{1/2} \end{aligned} \tag{21}$$

and

$$\frac{\mathrm{d}\xi\mathrm{d}\eta}{\mathrm{d}\hat{\xi}\mathrm{d}\hat{\eta}}=\frac{\left(\xi_{e+1}-\xi_e\right)\left(\eta_{e+1}-\eta_e\right)}{4} \tag{22}$$

Based on the local support property of NURBS basis functions, a set of local basis functions that are related to the global basis functions can be written as

$$N_d^e(\hat{\xi},\hat{\eta})\equiv R_{i,j}^{p,q}(\xi(\hat{\xi}),\eta(\hat{\eta})) \tag{23}$$

where d is the local basis function number. At this point, the information of any point in the element e can be expressed as

$$\begin{cases}\mathbf{x}(\hat{\xi},\hat{\eta})=\sum\limits_{d=1}^{(p+1)(q+1)}N_d^e(\hat{\xi},\hat{\eta})\mathbf{x}_d\\ T(\hat{\xi},\hat{\eta})=\sum\limits_{d=1}^{(p+1)(q+1)}N_d^e(\hat{\xi},\hat{\eta})T_d\\ Q(\hat{\xi},\hat{\eta})=\sum\limits_{d=1}^{(p+1)(q+1)}N_d^e(\hat{\xi},\hat{\eta})Q_d\\ \hat{T}_v(\hat{\xi},\hat{\eta})=\sum\limits_{d=1}^{(p+1)(q+1)}N_d^e(\hat{\xi},\hat{\eta})\hat{T}_{dv}^e\\ \hat{Q}_v(\hat{\xi},\hat{\eta})=\sum\limits_{d=1}^{(p+1)(q+1)}N_d^e(\hat{\xi},\hat{\eta})\hat{Q}_{dv}^e\end{cases} \tag{24}$$

Substituting Eq. (24) into Eq. (18), the 3D isogeometric dual reciprocity integration equation can be obtained in the following form

$$\begin{aligned}&C(\mathbf{x}_b)\sum_{d=1}^{(p+1)(q+1)}N_d^{e'}(\hat{\xi}',\hat{\eta}')T_d^{e'}(t)\\&\quad+\sum_{e=1}^{N_e}\sum_{d=1}^{(p+1)(q+1)}\left[\int_{-1}^{1}\int_{-1}^{1}Q^*\left(\mathbf{x}_b(\xi_b,\eta_b),\mathbf{x}(\hat{\xi},\hat{\eta})\right)N_d^e(\hat{\xi},\hat{\eta})J^e(\hat{\xi},\hat{\eta})\mathrm{d}\hat{\xi}\mathrm{d}\hat{\eta}\right]T_d^e(t)\\&\quad-\sum_{e=1}^{N_e}\sum_{d=1}^{(p+1)(q+1)}\left[\int_{-1}^{1}\int_{-1}^{1}T^*\left(\mathbf{x}_b(\xi_b,\eta_b),\mathbf{x}(\hat{\xi},\hat{\eta})\right)N_d^e(\hat{\xi},\hat{\eta})J^e(\hat{\xi},\hat{\eta})\mathrm{d}\hat{\xi}\mathrm{d}\hat{\eta}\right]Q_d^e(t)\\&=\sum_{v=1}^{N_t}\alpha_v\Bigg\{C(\mathbf{x}_b)\sum_{d=1}^{(p+1)(q+1)}N_d^{e'}(\hat{\xi}',\hat{\eta}')\hat{T}_{dv}^{e'}(\mathbf{x}_b\in\Gamma)\\&\quad+\sum_{e=1}^{N_e}\sum_{d=1}^{(p+1)(q+1)}\left[\int_{-1}^{1}\int_{-1}^{1}Q^*\left(\mathbf{x}_b(\xi_b,\eta_b),\mathbf{x}(\hat{\xi},\hat{\eta})\right)N_d^e(\hat{\xi},\hat{\eta})J^e(\hat{\xi},\hat{\eta})\mathrm{d}\hat{\xi}\mathrm{d}\hat{\eta}\right]\hat{T}_{dv}^e\\&\quad-\sum_{e=1}^{N_e}\sum_{d=1}^{(p+1)(q+1)}\left[\int_{-1}^{1}\int_{-1}^{1}T^*\left(\mathbf{x}_b(\xi_b,\eta_b),\mathbf{x}(\hat{\xi},\hat{\eta})\right)N_d^e(\hat{\xi},\hat{\eta})J^e(\hat{\xi},\hat{\eta})\mathrm{d}\hat{\xi}\mathrm{d}\hat{\eta}\right]\hat{Q}_{dv}^e\Bigg\}\end{aligned} \tag{25}$$

where $\mathbf{x}_b$ denotes the collocation point on the real boundary, ξ_b and η_b represent the local coordinate of the collocation point $\mathbf{x}_b$. In order to ensure that the positions of collocation points are on the real boundary in IGBEM, we use the Greville abscissae method [6] to generate the collocation points in parameter space. For example, the point (ξ_i',η_j') is defined by

$$\begin{cases}\xi_i'=\frac{\xi_{i+1}+\xi_{i+2}+\ldots+\xi_{i+p}}{p}\,i=1,2,\cdots,n\\ \eta_j'=\frac{\eta_{j+1}+\eta_{j+2}+\ldots+\eta_{j+q}}{q}\,j=1,2,\cdots,m\end{cases} \tag{26}$$

Using the first formula in Eq. (24), the corresponding collocation point position of ξ_i', η_j' in Eq. (26) can be obtained.

Note that $n\times m$ collocation points can be generated by Eq. (26). Applying these collocation points to Eq. (25), $n\times m$ linear equations can be obtained. Here, assuming the number of boundary collocation points is N_b, where $N_b=n\times m$. The definition of functions $\hat{T}_j$ and $\hat{q}_j$ in Eq. (18) involves N_t points $\mathbf{x}_j$, which need to be defined. Assuming N_t contains N_b points on the boundary and N_I points inside the domain, i.e. N_t=N_b + N_I. The following equation similar to Eq. (25) can be formed by applying N_I interior points:

$$\begin{aligned}&T(\mathbf{x}_I,t)+\sum_{e=1}^{N_e}\sum_{d=1}^{(p+1)(q+1)}\left[\int_{-1}^{1}\int_{-1}^{1}Q^*\left(\mathbf{x}_I,\mathbf{x}(\hat{\xi},\hat{\eta})\right)N_d^e(\hat{\xi},\hat{\eta})J^e(\hat{\xi},\hat{\eta})\mathrm{d}\hat{\xi}\mathrm{d}\hat{\eta}\right]T_d^e(t)\\&\quad-\sum_{e=1}^{N_e}\sum_{d=1}^{(p+1)(q+1)}\left[\int_{-1}^{1}\int_{-1}^{1}T^*\left(\mathbf{x}_I,\mathbf{x}(\hat{\xi},\hat{\eta})\right)N_d^e(\hat{\xi},\hat{\eta})J^e(\hat{\xi},\hat{\eta})\mathrm{d}\hat{\xi}\mathrm{d}\hat{\eta}\right]Q_d^e(t)\\&=\sum_{v=1}^{N_t}\alpha_v\Bigg\{\hat{T}_{uv}+\sum_{e=1}^{N_e}\sum_{d=1}^{(p+1)(q+1)}\left[\int_{-1}^{1}\int_{-1}^{1}Q^*\left(\mathbf{x}_I,\mathbf{x}(\hat{\xi},\hat{\eta})\right)\right.\\&\quad\left.\times N_d^e(\hat{\xi},\hat{\eta})J^e(\hat{\xi},\hat{\eta})\mathrm{d}\hat{\xi}\mathrm{d}\hat{\eta}\right]\hat{T}_{dv}^e(\mathbf{x}_I\in\Omega)\\&\quad-\sum_{e=1}^{N_e}\sum_{d=1}^{(p+1)(q+1)}\left[\int_{-1}^{1}\int_{-1}^{1}T^*\left(\mathbf{x}_I,\mathbf{x}(\hat{\xi},\hat{\eta})\right)N_d^e(\hat{\xi},\hat{\eta})J^e(\hat{\xi},\hat{\eta})\mathrm{d}\hat{\xi}\mathrm{d}\hat{\eta}\right]\hat{Q}_{dv}^e\Bigg\}\end{aligned} \tag{27}$$

Compared to Eq. (25), at these interior points, the jump term $C(\mathbf{x}_I)=1$ is satisfied.

For N_b boundary and N_I interior unknown quantities in Eqs. (25) and (27), we can solve the system of linear equations obtained by coupling Eqs. (25) and (27). Finally, N_t dimensional system of linear equations can be written in the matrix form as follows

$$\mathbf{HT}(t)-\mathbf{GQ}(t)=\sum_{v=1}^{N_t}\alpha_v\left(\mathbf{H}\hat{\mathbf{T}}_{\mathbf{v}}-\mathbf{G}\hat{\mathbf{Q}}_{\mathbf{v}}\right) \tag{28}$$

where the vector $\mathbf{T}(t)=\mathbf{T}$ can be expressed as

$$\mathbf{T}=\left[T_1T_2\cdots T_{N_b}T_{N_b+1}\cdots T_{N_t}\right]^{\mathrm{T}} \tag{29}$$

The first N_b elements in vector $\mathbf{T}$ denote the temperature coefficients of control points. The last N_I elements represent the temperature of the internal nodes. Vector $\mathbf{Q}(t)=\mathbf{Q}$ includes the N_b heat flux coefficients of control points that can be given by

$$\mathbf{Q}=\left[Q_1Q_2\cdots Q_{N_b}\right]^{\mathrm{T}} \tag{30}$$

The vectors $\hat{\mathbf{T}}_v$ in Eq. (28) can be written as

$$\hat{\mathbf{T}}_v=\left[\hat{T}_{1v},\hat{T}_{2v},\cdots,\hat{T}_{N_bv},\hat{T}_{(N_b+1)v},\cdots,\hat{T}_{N_tv}\right]^{\mathrm{T}} \tag{31}$$

where $\hat{T}_{lv}=\hat{T}_v(\mathbf{x}_l)$, $(l=1,2,\cdots,N_t)$, $\{\mathbf{x}_l\}_{l=1}^{N_t}$ represent the full set of points including boundary and interior points. The vectors $\hat{\mathbf{Q}}_v$ are written as

$$\hat{\mathbf{Q}}_v=\left[\hat{Q}_{1v},\hat{Q}_{2v},\cdots,\hat{Q}_{N_bv}\right]^{\mathrm{T}} \tag{32}$$

where $\hat{Q}_{lv}=\hat{Q}_v(\mathbf{x}_l)$, $(l=1,2,\cdots,N_b)$. Similar to Eqs. (29) and (30), the first N_b elements of vector $\hat{\mathbf{T}}_v$ and all elements of vector $\hat{\mathbf{Q}}_v$ indicate the control point coefficients corresponding to the function values of the distance between the boundary collocation points and point v. The last N_I elements of vector $\hat{\mathbf{T}}_v$ represent the function values of the distance from the interior points to point v.

To express facility, the matrices $\hat{\mathbf{T}}$ ($\hat{\mathbf{T}}\in\mathrm{R}^{N_t\times N_t}$) and $\hat{\mathbf{Q}}$ ($\hat{\mathbf{Q}}\in\mathrm{R}^{N_b\times N_t}$) containing vectors $\hat{\mathbf{T}}_v$ and $\hat{\mathbf{Q}}_v$ (as columns) are introduced, and time-dependent vector $\boldsymbol{\alpha}=\boldsymbol{\alpha}(t)$ ($\boldsymbol{\alpha}\in\mathrm{R}^{N_t\times1}$) is adopted which is used to rewrite the Eq. (13), applying at N_t points, i.e.

$$\boldsymbol{\alpha}=\mathbf{F}^{-1}\tilde{\mathbf{b}} \tag{33}$$

where $\mathbf{F}\in\mathrm{R}^{N_t\times N_t}$, $\tilde{\mathbf{b}}=\tilde{\mathbf{b}}(t)\in\mathrm{R}^{N_t\times1}$. Elements of matrix $\mathbf{F}$ are generated by

$$F_{lj}=f_j(\mathbf{x}_l),(l=1,2,\cdots,N_t) \tag{34}$$

where function f_j is given by Eq. (14). Vector $\tilde{\mathbf{b}}$ represents the right-hand side of Eq. (12), i.e. its elements at collocation points $\mathbf{x}_l$ can be written as

$$\tilde{b}_l=\frac{1}{\lambda}\frac{\partial T(\mathbf{x}_l,t)}{\partial t}-\frac{1}{k}g(\mathbf{x}_l,t),(l=1,2,\cdots,N_t) \tag{35}$$

Finally, Eq. (28) can be rewritten as

$$\mathbf{HT}(t)=\mathbf{GQ}(t)-\mathbf{C}\tilde{\mathbf{b}}(t) \tag{36}$$

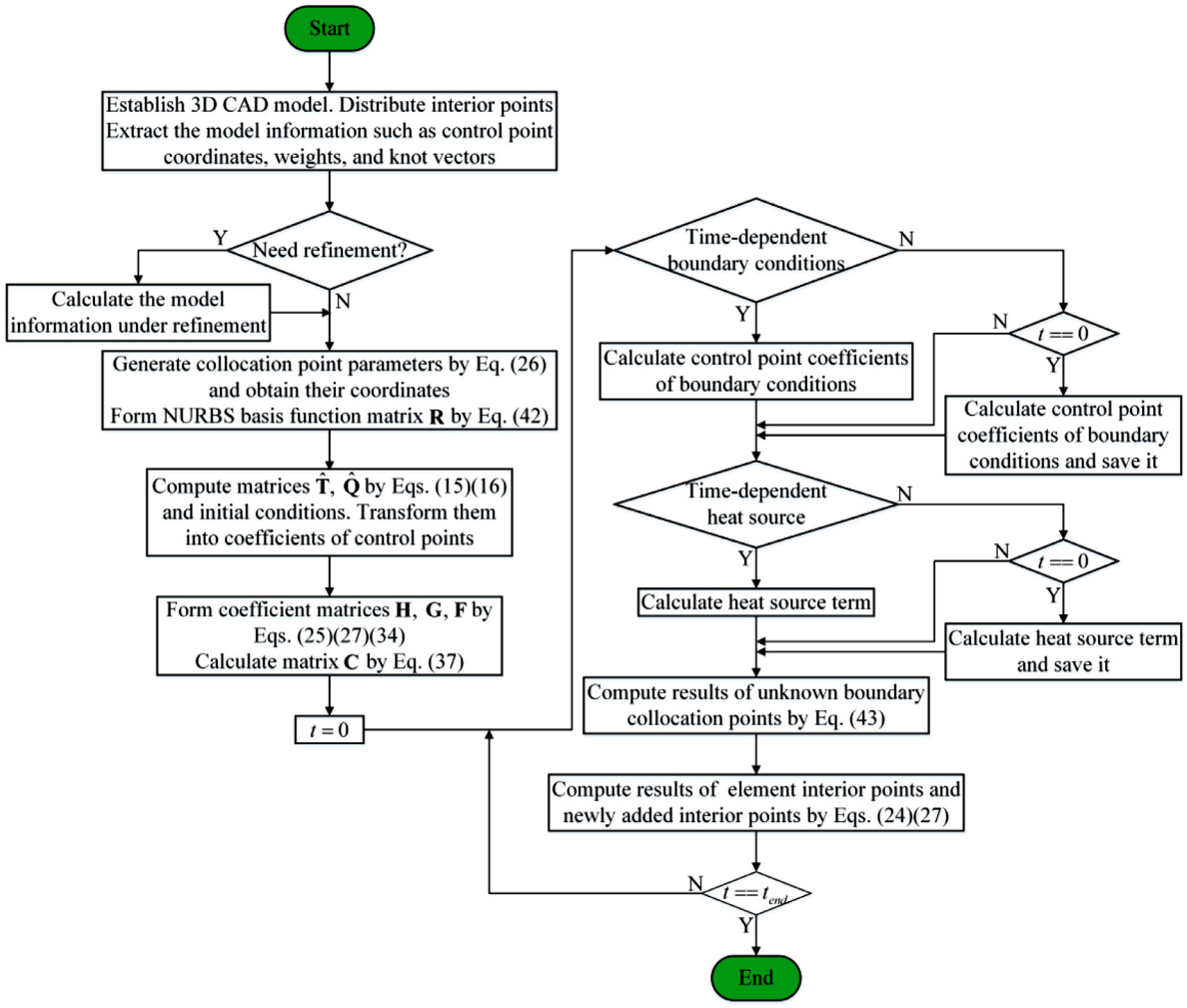

Fig. 1. Flow chart of IG-DRBEM.

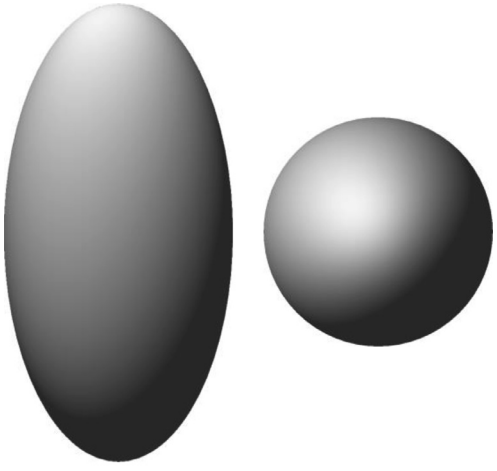

(a) Front view (b) Vertical view

Fig. 2. The isogeometric model of the ellipsoid with different viewing angles.

where

$$\mathbf{C} = -\left(\mathbf{H}\hat{\mathbf{T}} - \mathbf{G}\hat{\mathbf{Q}}\right)\mathbf{F}^{-1} \tag{37}$$

Note that Eq. (36) includes three time-dependent unknown vectors, namely $\mathbf{T}(t)$, $\mathbf{Q}(t)$ and $\tilde{\mathbf{b}}(t)$. In this paper, the two-level time integration scheme will be used to approximate these unknown vectors [14].

4.3. Two-level time integration

To facilitate subsequent expression, we will specify the following symbolic conventions. Δt denotes the time step size, $[t_s, t_{s+1}]$ represents the s-th time interval, all quantities computed at time t_s will be used by the superscript s. Based on the two-level time integration scheme, each element of vectors $\mathbf{T}(t)$, $\mathbf{Q}(t)$, and the heat source $g(t)$ can be approximated by a linear combination of values at t_s and t_{s+1} and three parameters θ_T, θ_Q, and θ_g, such as

$$\begin{cases} T_l = (1-\theta_T)T_l^s + \theta_T T_l^{s+1} \\ Q_l = (1-\theta_Q)Q_l^s + \theta_Q Q_l^{s+1} \\ g_l = (1-\theta_g)g_l^s + \theta_g g_l^{s+1} \\ \frac{\partial T_l}{\partial t} = \frac{T_l^{s+1} - T_l^s}{\Delta t} \end{cases}, (l = 1, 2, \cdots, N_t) \tag{38}$$

Based on this, the first N_b elements in vector $\tilde{\mathbf{b}}$ can be given by

$$\tilde{b}_l = \frac{1}{\lambda \Delta t}\sum_{i=1}^{n}\sum_{j=1}^{m} R_{i,j}^{p,q}(\xi,\eta)\left(T_{ij}^{s+1} - T_{ij}^{s}\right) - \left[(1-\theta_g)\frac{g_l^s}{k} + \theta_g \frac{g_l^{s+1}}{k}\right], (l = 1, 2, \cdots, N_b) \tag{39}$$

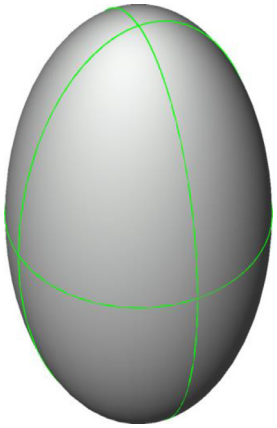

Fig. 3. The mesh of isogeometric model.

Table 1
The knot vector and the order of isogeometric ellipsoid model.

Direction	Order	Knot vector
ξ	$p = 2$	{0, 0, 0, 1, 1, 2, 2, 3, 3, 4, 4, 4}
η	$q = 2$	{0, 0, 0, 1, 1, 1}

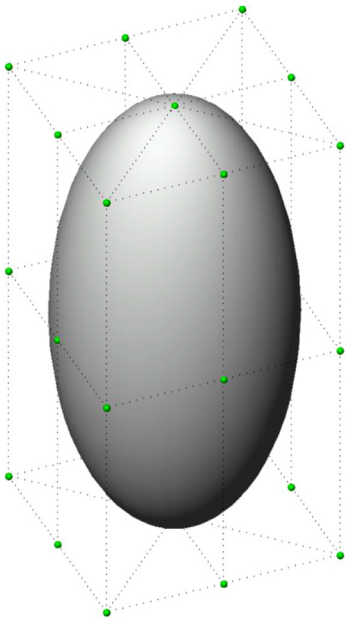

Fig. 4. The control point of the isogeometric model.

where (ξ, η) represents the corresponding parameter value of the boundary collocation point l in the knot vector space, T_{ij}^{s} and T_{ij}^{s+1} are the temperature coefficients of each boundary control point at the two-level time, g_l^s and g_l^{s+1} denote the heat source values of boundary collocation points at the two-level time, respectively. The last N_I elements can be expressed as

$$\tilde{b}_l = \frac{1}{\lambda\Delta t}\left(T_l^{s+1} - T_l^s\right) - \left[\left(1-\theta_g\right)\frac{g_l^s}{k} + \theta_g\frac{g_l^{s+1}}{k}\right], \quad (l = N_b+1, N_b+2, \cdots, N_t) \tag{40}$$

Note that T_l^s and T_l^{s+1} in Eq. (40) are the temperature of interior points rather than the temperature coefficients. Here, g_l^s and g_l^{s+1} are the heat source values of interior points. Combining Eq. (39) with Eq. (40),

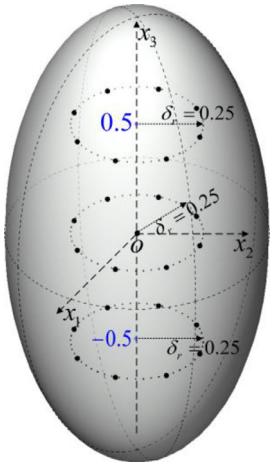

Fig. 5. The isogeometric model with 25 interior points.

Table 2
Results with different expansions of f_j.

f_j	Mabserr	Mrelerr (%)	e_{L_2}
(i)	0.005517	0.1136	4.5253e-04
(ii)	0.010684	0.2215	1.0885e-03
(iii)	0.041173	0.9166	4.6176e-03

Table 3
Results of different time steps.

Δt	Mabserr	Mrelerr (%)	e_{L_2}
0.25	0.014795	0.2676	1.4605e-03
0.1	0.005203	0.1077	4.3028e-04
0.05	0.005489	0.1130	4.4866e-04
0.01	0.005518	0.1136	4.5254e-04
0.001	0.005519	0.1137	4.5270e-04

the vector $\tilde{\mathbf{b}}$ can be written as

$$\tilde{\mathbf{b}} = \frac{1}{\lambda\Delta t}\mathbf{R}\left(\mathbf{T}^{s+1} - \mathbf{T}^s\right) - \frac{1}{k}\left[\left(1-\theta_g\right)\mathbf{g}^s + \theta_g\mathbf{g}^{s+1}\right] \tag{41}$$

where the matrix $\mathbf{R}$ is given by

$$\mathbf{R} = \begin{bmatrix} \left(\mathbf{R}_\Delta\right)_{N_b\times N_b} & \mathbf{0} \\ \mathbf{0} & \mathbf{I}_{N_I\times N_I} \end{bmatrix} \tag{42}$$

in which elements of $\mathbf{R}_\Delta$ are generated by the basis functions $R_{i,j}^{p,q}(\xi,\eta)$. For example, the element of row u and column v in $\mathbf{R}_\Delta$ is expressed as $(\mathbf{R}_\Delta)_{uv}$, then $(\mathbf{R}_\Delta)_{uv}$ is the function value obtained by substituting the parameter (ξ, η) of the u-th boundary collocation point in the knot vector space into the v-th NURBS basis function.

Substituting Eqs. (38) and (41) into Eq. (36), the solved equations can be given by

$$\left(\frac{1}{\lambda\Delta t}\mathbf{CR} + \theta_T\mathbf{H}\right)\mathbf{T}^{s+1} - \theta_Q\mathbf{G}\mathbf{Q}^{s+1} = \left[\frac{1}{\lambda\Delta t}\mathbf{CR} - \left(1-\theta_T\right)\mathbf{H}\right]\mathbf{T}^s + \left(1-\theta_Q\right)\mathbf{G}\mathbf{Q}^s + \frac{\mathbf{C}}{k}\left[\left(1-\theta_g\right)\mathbf{g}^s + \theta_g\mathbf{g}^{s+1}\right] \tag{43}$$

where $\mathbf{T}^s$ and $\mathbf{Q}^s$ are specified by the initial conditions or obtained by solving at previous time steps, some of $\mathbf{T}^{s+1}$ and $\mathbf{Q}^{s+1}$ can be given by the boundary conditions and the remaining terms can be solved at time t_{s+1}, and the heat source vectors $\mathbf{g}^s$ and $\mathbf{g}^{s+1}$ are evaluated by known heat source functions. It is noted that the matrices **C, R, H**, and **G** are only associated with spatial coordinates, so we only need to compute them once in the whole solving process. Similarly, the vectors $\mathbf{g}^s$ and $\mathbf{g}^{s+1}$ need to be evaluated once when the heat source function is time-independent. In addition, in order for the solving program to automatically start the calculation, θ_T, θ_Q, and θ_g are taken as 1 in the first time step and 0.5 in the remaining time steps.

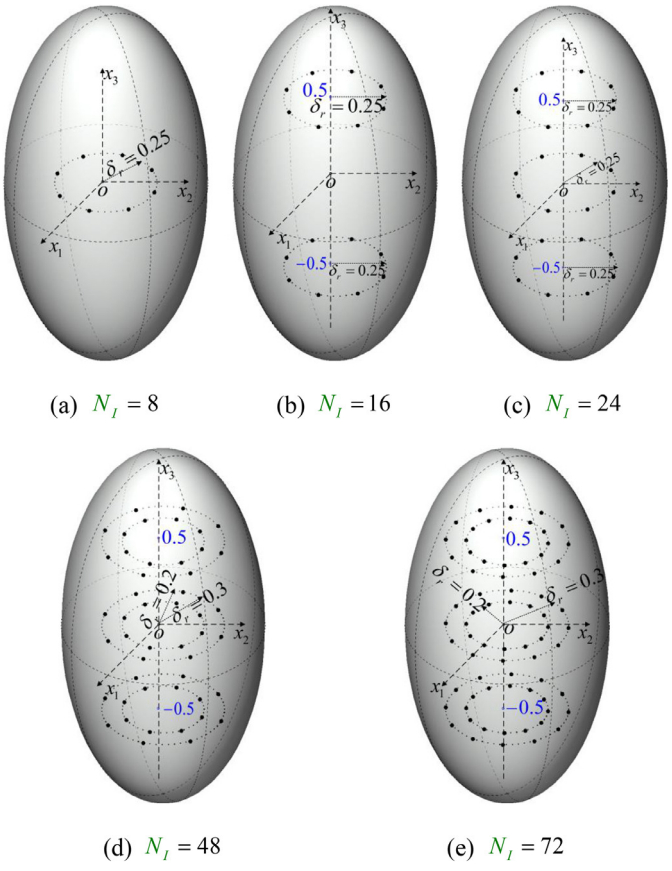

Fig. 6. The isogeometric model with regular distributed interior points.

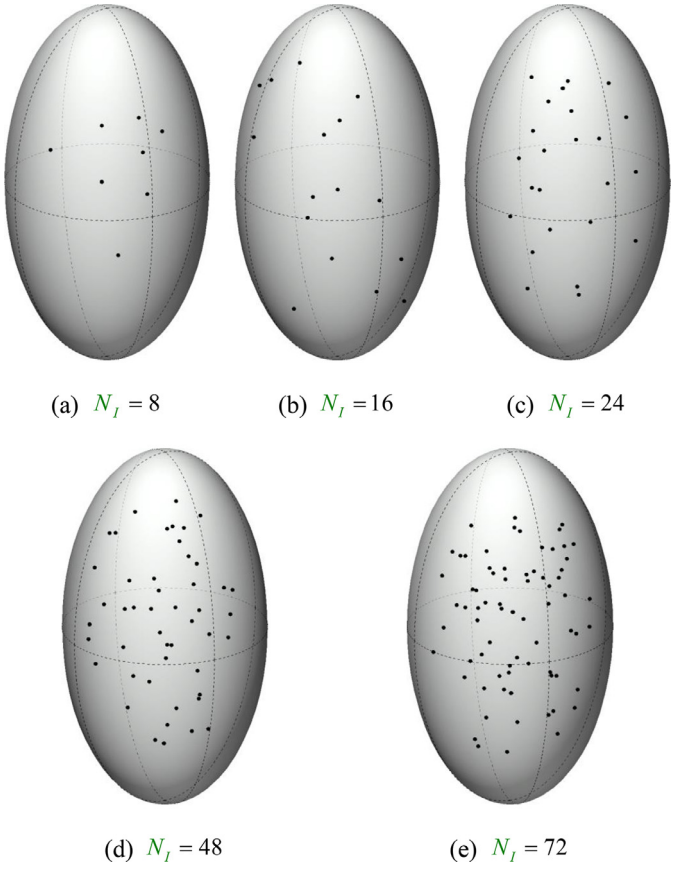

Fig. 7. The isogeometric model with random distributed interior points.

4.4. Integration schemes of different types

Similar to the conventional BEM, the regular, nearly singular, and singular integrals still have to be considered in IG-DRBEM, which is related to the accuracy of the unknown quantities. The regular integral denotes that the integrand is bounded and integrable. The nearly singular is the integrand with very large values, for example, the distance r is very small when the source and the field point are very close together. For the singular integral, the integrand trends to infinite when the source point and the field point coincide, $r = 0$. As described above, based on the theory of literature [24] in this work, here we continue to use the same scheme for solving the three kinds of integrals. Here we give only a brief introduction, and the detailed solving process can be referred to in literature [24].

(a) **Compute of regular and nearly singular integrals.** It is well known that surface geometry can be accurately described with only a few control points when the model is established with NURBS. For the IGBEM, the degree of freedom is reduced, but the element size is relatively large. If the number of numerical integration points is specified, the calculation accuracy for different elements may be lost, or the calculation cost may be increased. To guarantee numerical integration accuracy, it is necessary to use the adaptive integration scheme to solve different integrals. In this paper, an adaptive integration scheme is used to solve regular integrals and nearly singular integrals by means of the element sub-division technique [23,36].

(b) **Evaluation of boundary singular integrals.** First, the RIM is used to transform the singular integral on the element into a contour integral along the four sides of the element. Then, the power series expansion method [33] is used to solve the singular integral in IG-DRBEM, where the singularities involved in integration kernels can be analytically removed by expressing the nonsingular parts of the integration kernels as polynomials of the distance r.

4.5. Evaluation of temperature at any point in the element and domain

In general, when using NURBS to generate 3D surface geometry, a few control points can accurately describe the geometry. At the same time, in order to maintain a certain accuracy, a few interior points are selected in the domain. After the corresponding coefficients of the control points and the unknown quantities in the domain are solved, if we want to obtain the temperature field at any point in the surface element and any point in the domain at different time steps, we can solve it through Eqs. (24) and (27).

The detailed flow chart of IG-DRBEM is shown in Fig. 1.

5. Numerical examples

In order to verify the performance of the presented method, the absolute error (Abserr) $|\mathbf{T}_{ref} - \mathbf{T}_{num}|$, the relative error (Relerr) $100 \times |\mathbf{T}_{ref} - \mathbf{T}_{num}|/\mathbf{T}_{ref}$, and the relative L_2 error norm in temperatures e_{L_2} which evaluates the overall error, are used in the following numerical examples, where

$$e_{L_2} = \frac{\left\|\mathbf{T}_{ref} - \mathbf{T}_{num}\right\|_{L_2}}{\left\|\mathbf{T}_{ref}\right\|_{L_2}} \tag{44}$$

in which

$$\left\|\mathbf{T}_{ref}\right\|_{L_2} = \sqrt{\sum_{i=1}^{N_t} T_i^2} \tag{45}$$

The physical parameters k, ρ, and c are all set to 1 in all the examples.

Table 4
e_{L_2} using different numbers of interior points at $t = 0.5$.

N_I	Regular	Random
8	2.77e-4	2.09e-4
16	3.72e-4	3.66e-4
24	4.47e-4	4.10e-4
48	5.34e-4	5.28e-4
72	5.53e-4	5.50e-4

5.1. An ellipsoid model

Similar to the example in [24], an ellipsoid which is given by $4x_1^2 + 4x_2^2 + x_3^2 = 1$ with the temperature boundary condition, is considered without heat sources to test the effect of the expansion function f_j, the time step Δt, the number of interior points, and the minimum distance δ_{md} between the inner point and the boundary. The initial condition and the exact solution are given by $T_0 = e^{x_1} + e^{x_2} + e^{x_3}$ and $T = e^{x_1+t} + e^{x_2+t} + e^{x_3+t}$, respectively. The isogeometric model of the ellipsoid is shown in Fig. 2 from different viewing angles. In this example, as shown in Fig. 3, 8 sparse isogeometric elements are applied to solve the temperature field at $t = 0.5$. The knot vector and the order used NURBS are given in Table 1. 26 control points are adopted as shown in Fig. 4.

(A) The effect of different approximation functions f_j

In this case, $\Delta t = 0.01$ is used and the three expansion forms are considered as follows

(i) $f_j = 1 + r_j$
(ii) $f_j = 1 + r_j + r_j^2$
(iii) $f_j = 1 + r_j + r_j^2 + r_j^3$

As shown in Fig. 5, 25 interior points are distributed into three planes $x_3 = \pm 0.5$ and $x_3 = 0$ which parallel to the plane x_1ox_2 in the ellipsoid domain, where 8 interior points are respectively distributed on the circumference of 0.25 away from the x_3-axis, and an interior point is placed at the geometric center (0, 0, 0).

From the maximum absolute error (Mabserr), the maximum relative error (Mrelerr), and e_{L_2} given in Table 2, we can see that the results obtained by the expression (i) have the highest accuracy. Based on this, the expression (i) will be used to compute in the subsequent examples.

(A) The effect of different time steps

In this part, we consider the effect of different time steps on the calculated results. The isogeometric calculation information used is the same as part (A). Note that the approximation function is taken as $f_j = 1 + r_j$.

It can be seen from Table 3 that numerical results tend to be stable and the accuracy is improved as the time step decreases, especially when $\Delta t \le 0.05$. The Mabserr and the Mrelerr are not more than 0.0055 and 0.11 respectively, and e_{L_2} is basically controlled at the magnitude of 10^{-4}. In order to reduce the influence of time step on the calculated results, $\Delta t = 0.01$ is adopted in subsequent examples.

(A) The effect of the number of interior points

In this part, five groups with different numbers of interior points are regularly distributed into different planes perpendicular to the x_3-axis. The first group (Fig. 6 (a)) of 8 interior points are distributed on plane $x_3 = 0$, where these points are uniformly distributed on the circumference of 0.25 from the x_3-axis, here we use δ_r to express the distance, namely $\delta_r = 0.25$. The second group (Fig. 6 (b)) of 16 interior points are distributed on planes $x_3 = \pm 0.5$, where $\delta_r = 0.25$. For the third group (Fig. 6 (c)), in addition to containing the same number of interior points as the second group, it also includes 8 interior points distributed into plane $x_3 = 0$. As shown in Fig. 6 (d) and (e), the remaining groups of interior points are uniformly distributed into the planes $x_3 = 0$ and $x_3 = \pm 0.5$, where $\delta_r = 0.2$ and $\delta_r = 0.3$. In addition, five groups of randomly distributed interior points are also discussed such as $N_I = 8$, 16, 24, 48, and 72, as shown in Fig. 7.

It can be seen from Table 4 that the magnitude of e_{L_2} error can reach 10^{-4} with distributed regular and random interior points. The e_{L_2} errors at randomly distributed interior points are slightly smaller than using regularly distributed interior points. But as the number of interior points increases, the e_{L_2} errors tend to stabilize. Therefore, in order to obtain more accurate results, a small number of interior points need to be distributed as uniformly as possible within the domain when IG-DRBEM is used.

Table 5
Temperatures with different δ_{md}.

Coordinate of interior point	δ_{md}	IG-DRBEM	Exact	Relerr(%)
(0, 0,0)	0.5	4.9450	4.9461	0.023
(0.4, 0, 0)	0.1	5.7528	5.7570	0.074
(0.49, 0, 0)	0.01	5.9847	5.9886	0.066
(0.499, 0, 0)	0.001	6.0103	6.0130	0.044
(0, 0.4, 0)	0.1	5.7527	5.7570	0.074
(0, 0.49, 0)	0.01	5.9846	5.9886	0.066
(0, 0.499, 0)	0.001	6.0103	6.0130	0.044
(0, 0, 0.9)	0.1	7.3431	7.3526	0.12
(0, 0, 0.99)	0.01	7.7309	7.7345	0.046
(0, 0, 0.999)	0.001	7.7747	7.7746	0.0006

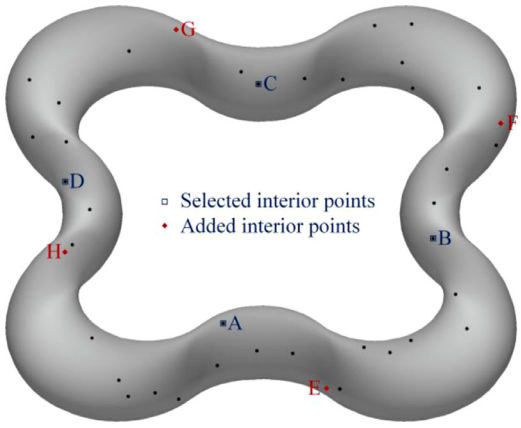

Fig. 8. The circular pipe model.

Table 6
The knot vector and the order of circular pipe model.

Direction	Order	Knot vector
ξ	$p = 2$	{0, 0, 0, 1, 1, 2, 2, 3, 3, 4, 4, 5, 5, 6, 6, 7, 7, 8, 8, 9, 9, 10, 10, 11, 11, 12, 12, 12}
η	$q = 2$	{0, 0, 0, 1, 1, 2, 2, 3, 3, 4, 4, 4}

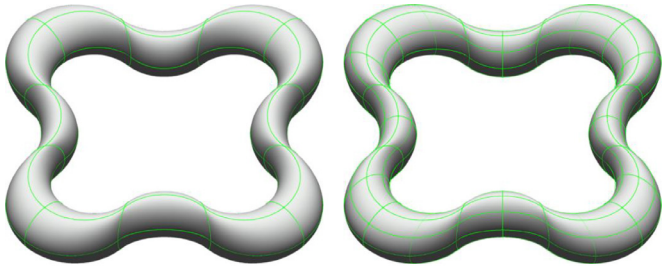

(a) Ref=0 (b) Ref=1

Fig. 9. Different element divisions of circular pipe model.

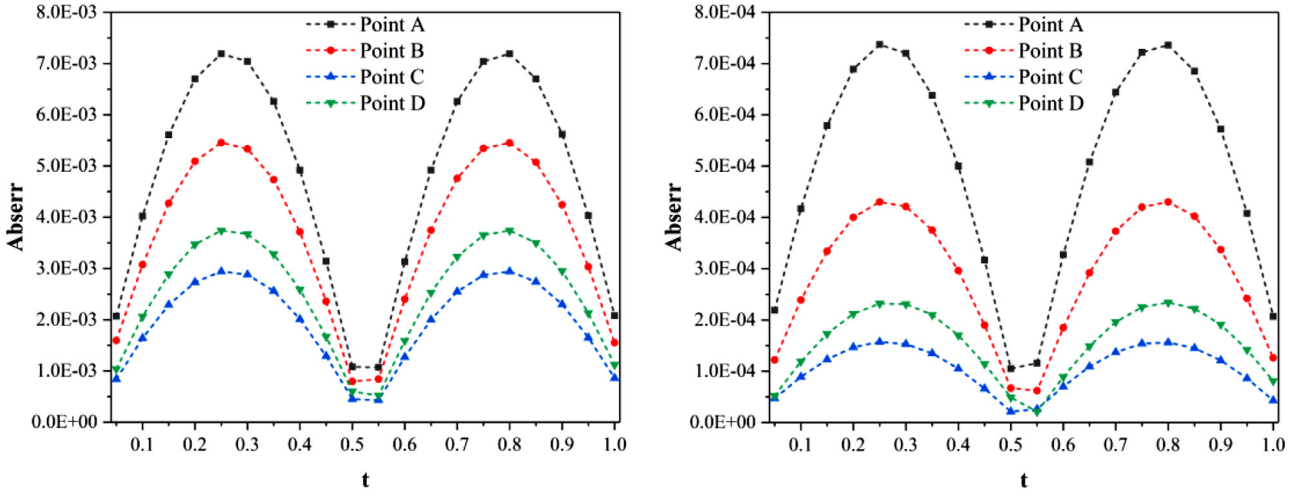

Fig. 10. Absolute errors of selected interior points.

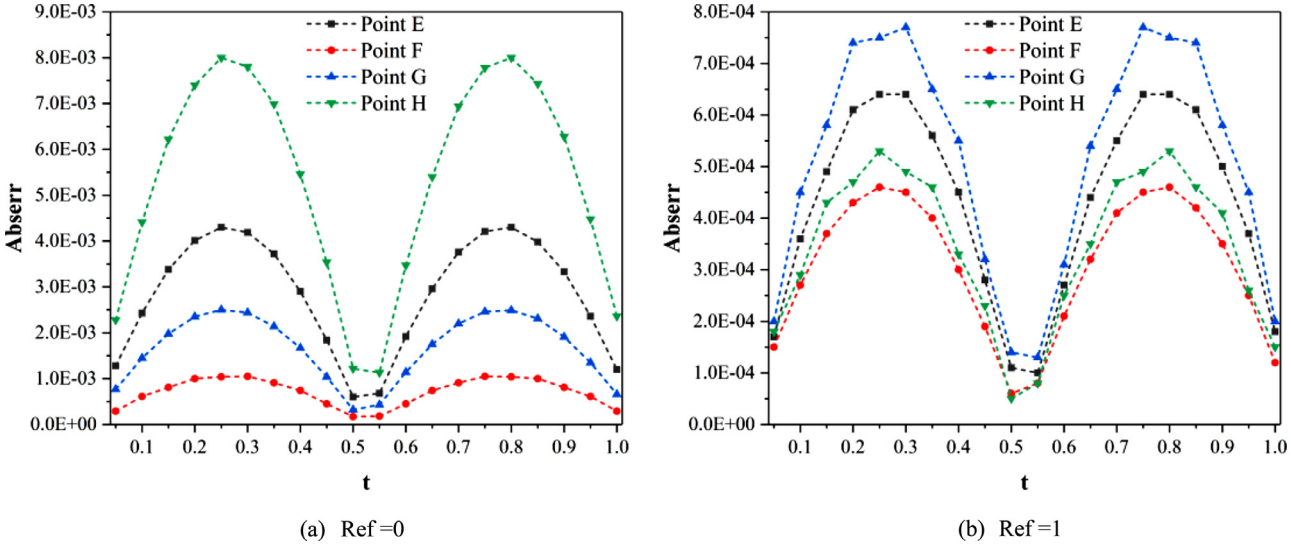

Fig. 11. Absolute errors of added interior points.

Table 7
Computational information of model and temperature e_{L_2} at $t = 1$; t_{RIM}: time for RIM to calculate singular integrals and t_{SUM}: total computation time.

Case	N_b	N_I	N_t	N_{AI}	e_{L_2}	t_{RIM}/t_{SUM}
(a)	192	36	228	4	3.56E-3	85.13%
(b)	432	36	468	4	3.95E-4	64.84%

(A) The effect of the minimum distance δ_{md} between the interior point and the boundary

In this part, only one interior point is distributed into the domain. Because the denominator of the fundamental solution of the three-dimensional potential problem used in this paper is a function of distance. When the boundary integral is calculated, the smaller distance between the interior point and the boundary will cause the greater singularity of the nearly singular integral. In order to verify the effect of the minimum distance δ_{md} from the interior point to the boundary and the performance of the adaptive integration method in IG-DRBEM, we make the point (0, 0, 0) gradually approach the ellipsoid boundary along the directions of coordinate axes x_1, x_2 and x_3, respectively. It can be seen from Table 5 that the maximum relative error is no more than 0.1%. Even when δ_{md}=0.001, the relative errors are basically controlled within 0.04%. Thus, the present method deals well with nearly singular integrals. In addition, it can be seen from the comparison with part (B) that larger relative errors are caused when more interior points are distributed. According to previous studies such as references [21] and [37], this is the normal situation for DRBEM.

5.2. A circular pipe model

In this example, a 3D geometry with 36 interior points is considered as shown in Fig. 8, where the knot vector information is presented in Table 6. The initial temperature and the temperature boundary condition can be specified by the exact expression of the temperature field,

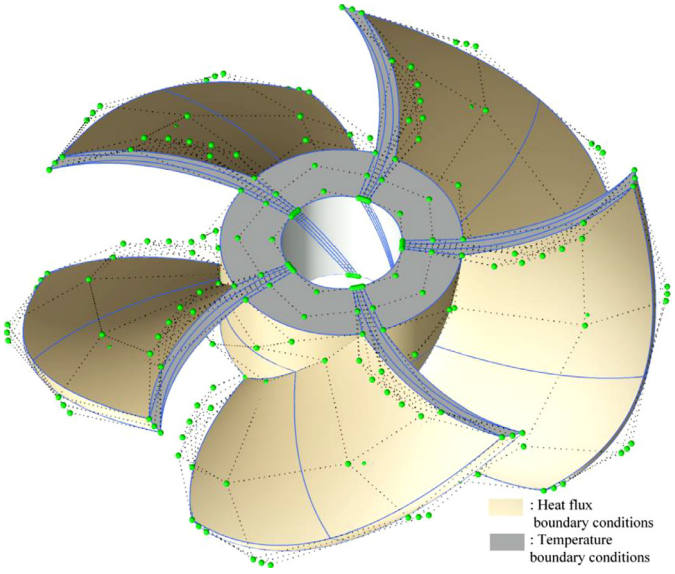

Fig. 12. The computational model of propeller.

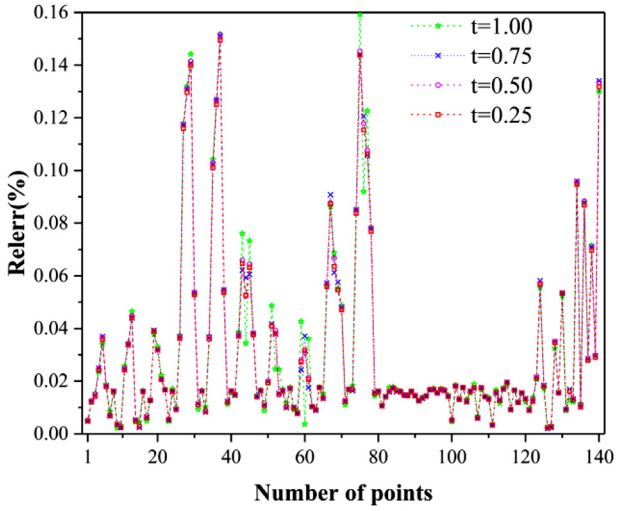

Fig. 13. Results of the collocation points on the boundary and the interior points in the domain.

namely $T = (x_1{}^2 + 2x_2{}^2 - 3x_3{}^2)\sin(6t)$. The heat source can be expressed as $g = 6(x_1{}^2 + 2x_2{}^2 - 3x_3{}^2)cos(6t)$.

As shown in Fig. 9, 48 and 192 surface elements are adopted by means of different refinements (Ref). The computational information of the model is shown in Table 7. To show the accuracy of interior points calculation, four interior points are randomly selected from 36 interior points of the IG-DRBEM calculation model, such as A (0.8071, 0.5127, 0.1666), B (-0.6598, 0.6785, -0.2041), C (-0.6954, -0.7156, -0.0835), and D (0.5272, -0.9969, -0.1281). The calculation results are presented in Fig. 10. It can be seen that the temperatures at four points when Ref=1 are more accurate than when Ref=0. In fact, when the element has not been refined, i.e. Ref=0, the calculated results are relatively accurate, where the Mabserr can reach the 10^{-3} magnitude. In addition, to evaluate the overall temperature error of the calculation model and the computational cost of using RIM to calculate singular integrals. The temperatures e_{L_2} for all nodes and the percentage of CPU time used by the RIM to calculate the singular integrals are shown in Table 7. We can find that the precision of temperature field calculation can be improved by element refinement, and in order to obtain accurate singular integral results, RIM occupies a large part of the total computation time.

Usually, a small number of interior points are required in order to compute the domain integral in DRM. However, it is necessary to study the temperature field at any location in the domain. Here, we can still use the idea of the traditional boundary element method. After solving Eq. (36), we use Eq. (27) to calculate the temperature of any inner point. As shown in Fig. 8, the temperatures of four newly added internal points (N_{AI}) such as E (0.5444, 1.0534, -0.1590), F (-1.4860, 0.3785, -0.1631), G (-0.5599, -1.2205, 0.0726), H (1.0349, -0.4924, 0.1201) are computed. It can be seen from Fig. 11 that the temperature of the newly added interior points has the same precision as that of the four randomly selected points.

5.3. A propeller

As shown in Fig. 12, a propeller is considered with 100 elements, 360 collocation points, and 60 interior points, where the temperature boundary condition and heat flux boundary condition have been marked in geometry. The boundary conditions are given by the exact solution $T = 100(\cos(x_1) + cos(x_2) + cos(x_3))e^{-t}$. The knot vector information of the model is shown in Table 8.

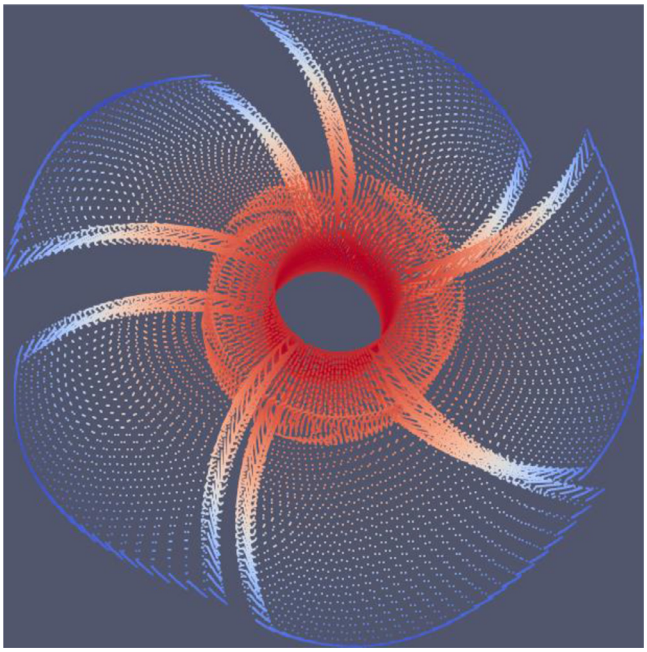

Fig. 14. Calculated interior points in all elements.

Table 8
The knot vector of propeller.

Direction	Order	Knot vector
ξ	$p = 2$	{0, 0, 0, 1, 1, 2, 2, 3, 3, 4, 4, 5, 5, 6, 6, 7, 7, 8, 8, 9, 9, 10, 10, 11, 11, 12, 12, 13, 13, 14, 14, 15, 15, 16, 16, 17, 17, 18, 18, 19, 19, 20, 20, 20}
η	$q = 2$	{0, 0, 0, 0.5, 1, 1, 2, 2, 3, 3, 4, 4, 4}

As shown in Fig. 13, the relative errors of unknown temperature results of boundary and in-domain nodes are not more than 0.16%. In order to present the result accuracy of temperature distribution better on the entire geometric surface, based on the numerical results of 100 sparse elements, NURBS interpolation calculations are carried out for the distributed internal nodes of the whole propeller elements. Finally, a total of 46080 points are calculated as shown in Fig. 14. It can be seen

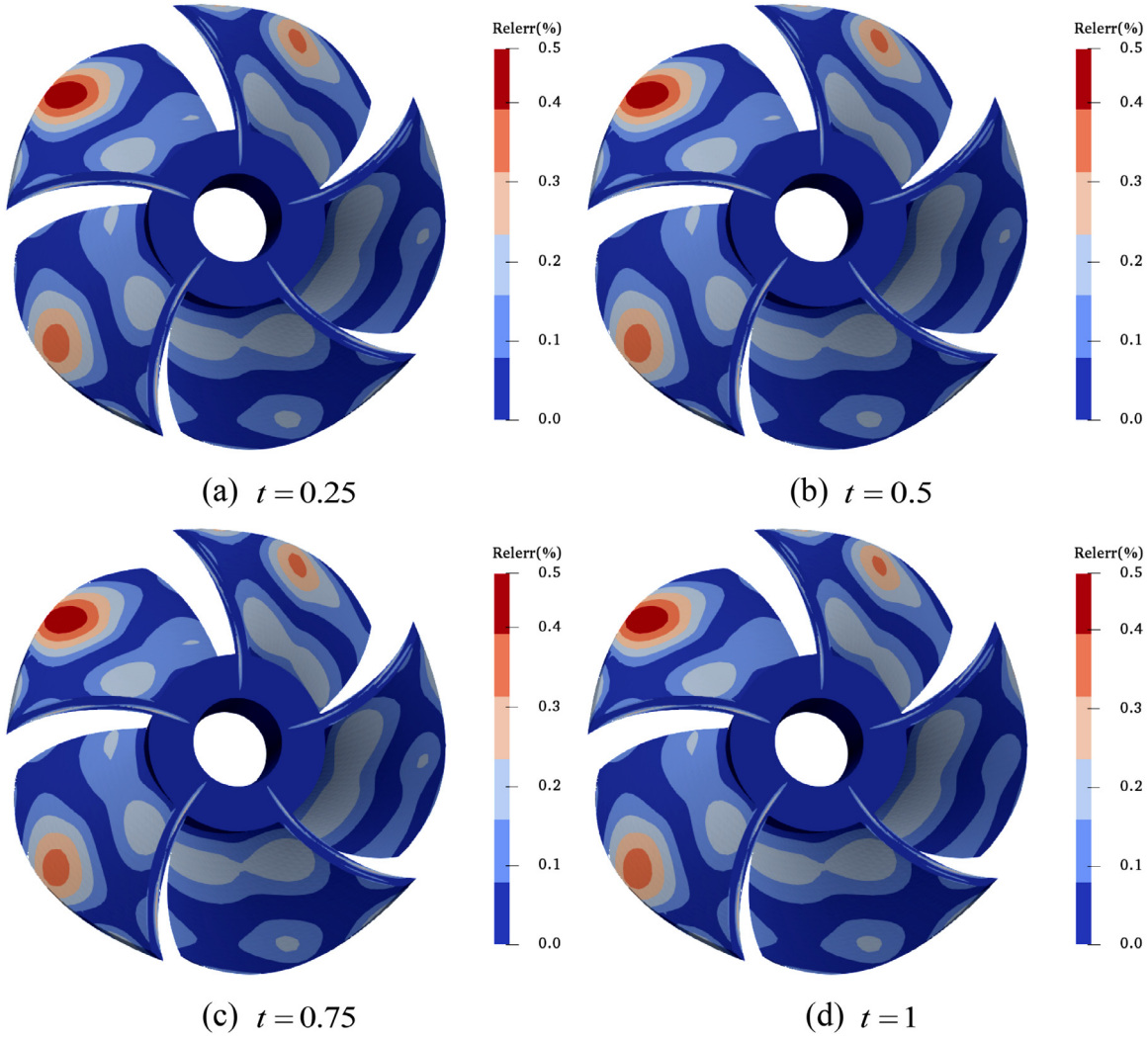

Fig. 15. Relative errors contour of all points.

from Fig. 15 that the Mrelerrs are all less than 0.5% at different times. Also, the relative error distribution is relatively stable at different times. Therefore, using sparse NURBS element information and solved results, we can still obtain relatively accurate numerical results by means of NURBS interpolation.

6. Conclusions

In this paper, the IG-DRBEM is applied to solve the 3D transient heat transfer problem. It gives full play to the convenience of the DRM in the transformation of domain integration and the high symmetry of formula expression. The results show that the high precision temperature field with complex geometry can be obtained by IG-DRBEM. The temperature field inside the element is computed by the NURBS interpolation using obtained information of the element control points. Similar to the traditional BEM, based on the known and solved information of control and interior points, the temperature of any interior point is computed. The numerical results show that the present scheme can obtain satisfactory results. The work in this paper can extend the application category of IGBEM to some extent. In particular, the adaptive integration scheme for regular integrals and the coupling method with the RIM and power series expansion method for singular integrals make the proposed method have good adaptability to the shape of elements. It can establish a foundation for solving time-dependent optimization and thermodynamic coupling problems. Furthermore, the examples in this paper are single-patch modeling, and the complex model can be realized by increasing the number of control points and adjusting the positions and weights of control points based on simple NURBS geometry such as ellipsoid. However, because single-patch NURBS uses only a set of knot vectors and control points, there are still many complex models that cannot be implemented. To overcome this limitation, multi-patch modeling analysis will be considered as soon as possible in the future. In addition, the same basis function such as NURBS is adopted to approximate the field variables and describe the geometry. In order to solve the complex geometry with dramatically varying boundary conditions, the different approximate functions for describing filed variables and geometry information will be considered in the future.

Declaration of Competing Interest

The authors declare that they have no known competing financial interests or personal relationships that could have appeared to influence the work reported in this paper.

Acknowledgement

The research was supported by the National Natural Science Foundation of China (No. 11872166, 12002009), the International Postdoctoral Exchange Fellowship Program of China (No. 20180096), and China

Postdoctoral Science Foundation (No. 2016M592042). Thanks to Elena Atroshchenko, senior lecturer at the University of New South Wales, for your valuable suggestions, especially when we begin to study IGBEM.

References

[1] Hughes TJ, Cottrell JA, Bazilevs Y. Isogeometric analysis: CAD, finite elements, NURBS, exact geometry and mesh refinement. Comput Methods Appl Mech Engrg 2005;194:4135–95.

[2] Auricchio F, Da Veiga LB, Hughes TJR, Reali A, Sangalli G. Isogeometric collocation methods. Math Models Methods Appl Sci 2010;20(11):2075–107.

[3] Moosavi MR, Khelil A. Isogeometric meshless finite volume method in nonlinear elasticity. Acta Mech 2015;226(1):123–35.

[4] Lin G, Zhang Y, Hu ZQ, Zhong H. Scaled boundary isogeometric analysis for 2D elastostatics. Sci China-Phys Mech Astron 2014;57(2):286–300.

[5] Natarajan S, Wang J, Song C, Birk C. Isogeometric analysis enhanced by the scaled boundary finite element method. Comput Methods Appl Mech Engrg 2015;283:733–62.

[6] Simpson RN, Bordas SPA, Trevelyan J, Rabczuk T. A two-dimensional isogeometric boundary element method for elastostatic analysis. Comput Methods Appl Mech Engrg 2012;209:87–100.

[7] Scott MA, Simpson RN, Evans JA, Lipton S, Bordas SP, Hughes TJR, Sederberg TW. Isogeometric boundary element analysis using unstructured T-splines. Comput Methods Appl Mech Engrg 2013;254:197–221.

[8] Peake MJ, Trevelyan J, Coates G. Extended isogeometric boundary element method (XIBEM) for two-dimensional Helmholtz problems. Comput Methods Appl Mech Engrg 2013;259:93–102.

[9] Takahashi T, Matsumoto T. An application of fast multipole method to isogeometric boundary element method for Laplace equation in two dimensions. Eng Anal Bound Elem 2012;36(12):1766–75.

[10] Nguyen BH, Tran HD, Anitescu C, Zhuang X, Rabczuk T. An isogeometric symmetric Galerkin boundary element method for two-dimensional crack problems. Comput Methods Appl Mech Engrg 2016;306:252–75.

[11] Peng X, Atroshchenko E, Kerfriden P, Bordas SPA. Isogeometric boundary element methods for three dimensional static fracture and fatigue crack growth. Comput Methods Appl Mech Engrg 2017;316:151–85.

[12] An Z, Yu T, Bui TQ, Wang C, Trinh NA. Implementation of isogeometric boundary element method for 2D steady heat transfer analysis. Adv Eng Softw 2018;116:36–49.

[13] Chen LL, Lian H, Liu Z, Chen HB, Atroshchenko E, Bordas SPA. Structural shape optimization of three dimensional acoustic problems with isogeometric boundary element methods. Comput Methods Appl Mech Engrg 2019;355:926–951.

[14] Nardini D, Brebbia CA. A new approach to free vibration using boundary elements. Bound Elem Methods Engrg 1982.

[15] Gao XW. The radial integration method for evaluation of domain integrals with boundary-only discretization. Eng Anal Bound Elem 2002;26(10):905–16.

[16] Wrobel LC, Brebbia CA. The dual reciprocity boundary element formulation for nonlinear diffusion problems. Comput Methods Appl Mech Engrg 1987;65(2):147–164.

[17] Lu WQ, Liu J, Zeng Y. Simulation of the thermal wave propagation in biological tissues by the dual reciprocity boundary element method. Eng Anal Bound Elem 1998;22(3):167–74.

[18] Albuquerque EL, Sollero P, Fedelinski P. Dual reciprocity boundary element method in Laplace domain applied to anisotropic dynamic crack problems. Comput Struct 2003;81(17):1703–13.

[19] Yu B, Zhou HL, Chen HL, Tong Y. Precise time-domain expanding dual reciprocity boundary element method for solving transient heat conduction problems. Int J Heat Mass Transfer 2015;91:110–18.

[20] Gomes G, Neto AMD, Bezerra LM, Silva R. An object-oriented approach to dual reciprocity boundary element method applied to 2D elastoplastic problems. Multi Model Mat Str 2019;15(5):958–74.

[21] Yu B, Cao G, Huo WD, Zhou HL, Atroshchenko E. Isogeometric dual reciprocity boundary element method for solving transient heat conduction problems with heat sources. J Comput Appl Math 2021;385:113197.

[22] Gong YP, Dong CY. An isogeometric boundary element method using adaptive integral method for 3D potential problems. J Comput Appl Math 2017;319:141–58.

[23] Gao XW, Davies TG. Boundary element programming in mechanics. Camberidge University Press; 2002.

[24] Gong YP, Dong CY. An isogeometric boundary element method using adaptive integral method for 3D potential problems. J Comput Appl Math 2017;319:141–58.

[25] Zhang YM, Gong YP, Gao XW. Calculation of 2D nearly singular integrals over high-order geometry elements using the sinh transformation. Eng Anal Bound Elem 2015;60:144–53.

[26] Xie GZ, Zhang JM, Dong YQ, Huang C, Li GY. An improved exponential transformation for nearly singular boundary element integrals in elasticity problems. Int J Solids Struct 2014;51(6):1322–9.

[27] Gu Y, Hua Q, Chen W, Zhang C. Numerical evaluation of nearly hyper-singular integrals in the boundary element analysis. Comput Struct 2016;167:15–23.

[28] Qin XY, Zhang JM, Xie GZ, Zhou FL, Li GY. A general algorithm for the numerical evaluation of nearly singular integrals on 3D boundary element. J Comput Appl Math 2011;235:4174–86.

[29] Telles JCF. A self-adaptive coordinate transformation for efficient numerical evaluation of general boundary element integrals. Internat J Numer Methods Engrg 1987;24:959–73.

[30] Karami G, Derakhshan D. An efficient method to evaluate hyper singular and super singular integrals in boundary integral equations analysis. Eng. Anal. Bound. Elem. 1999;23(4):317–26.

[31] Niu ZR, Zhou HL. A novel boundary integral equation method for linear elasticity–natural boundary integral equation. Acta Mech Solida Sin 2001;14(1):1–10.

[32] Wang J, Tsay TK. Analytical evaluation and application of the singularities in boundary element method. Eng Anal Bound Elem 2005;29(3):241–56.

[33] Gao XW. An effective method for numerical evaluation of general 2D and 3D high order singular boundary integrals. Comput Methods Appl Mech Engrg 2010;199(45):2856–64.

[34] Hahn DW, Özisik MN. Heat conduction. John Wiley & Sons; 2012.

[35] Nardini D, Brebbia CA. A new approach to free vibration analysis using boundary elements. Appl Math Model. 1983;7(3):157–62.

[36] Gao XW, Davies TG. Adaptive integration in elastoplastic boundary element analysis. J Chin Inst Eng 2000;23(3):349–56.

[37] Partridge PW, Brebbia CA, Wrobel LC. The dual reciprocity boundary element method. Southampton Boston: Computational Mechanics Publications; 1992.